Journal of Catalysis 268 (2009) 131–141

Contents lists available at ScienceDirect

Journal of Catalysis

journal homepage: www.elsevier.com/locate/jcat

Influence of step sites in the molecular mechanism of the water gas shift reaction catalyzed by copper

José L.C. Fajín [a], M. Natália D.S. Cordeiro [a], Francesc Illas [b,*], José R.B. Gomes [c,*]

[a] REQUIMTE, Faculdade de Ciências, Universidade do Porto, P-4169-007 Porto, Portugal
[b] Departament de Química Física & Institut de Química Teòrica i Computacional (IQTCUB), Universitat de Barcelona, C/Martí i Franquès 1, 08028 Barcelona, Spain
[c] CICECO, Departamento de Química, Universidade de Aveiro, 3810-193 Aveiro, Portugal

ARTICLE INFO

Article history:
Received 31 July 2009
Revised 10 September 2009
Accepted 12 September 2009
Available online 14 October 2009

Keywords:
Water gas shift
Cu
Low coordinate sites
DFT

ABSTRACT

The role of the step sites in the water gas shift reaction catalyzed by Cu surfaces has been studied by using the Cu(3 2 1)-stepped surface as a representative model and periodic density functional theory within a supercell approach. Several reaction pathways were considered and the corresponding transition states for the elementary steps on each pathway were located and characterized. It was found that the presence of steps favors the associative route through the carboxyl intermediate assisted by co-adsorbed OH. The presence of step sites decreases the activation energy barriers for the rate-limiting steps, compared to the perfect Cu(1 1 1) surface. Reaction rate constants for the different pathways involved in the two molecular mechanisms, obtained from transition state theory, are reported. Finally comparison to previous work allows one to propose a useful Brønsted–Evans–Polanyi relationship.

1. Introduction

Most of the hydrogen used in industry is produced from crude oil reforming, coal, natural gas, wood, and biomass [1]. However, the gas stream thus produced contains ~10% of CO which may degrade the performance of the catalysts used in the subsequent industrial processes. In particular, CO strongly poisons the Pt electrode used in the fuel cell systems [2] and, hence, must be necessarily removed from the gas stream before it enters the fuel cell system. This is usually achieved by means of the water gas shift (WGS) reaction ($CO + H_2O \rightarrow CO_2 + H_2$) in practice carried out in industry [3] using Cu [4] or Au [5–7] based catalysts. The WGS reaction is employed not only in the purification of the hydrogen-rich gas stream used in the fuel cells [8] but also in other important industrial processes such as the methanol synthesis [9] and the methanol steam reforming process [10].

It is generally accepted that the noble metal (Cu or Au) of the catalyst used in the WGS reaction constitutes the catalyst active phase [11–13], although other factors such as the nature of the support [5,14–17], the existence of oxygen vacancies [18,19], and the catalyst preparation process [20] may significantly affect the catalytic activity and the overall catalyst performance. Furthermore, subtle modifications of the catalyst by doping with traces of other metals [21,22] or by formation of alloys [23,24] have been found to considerably improve the catalytic performance. Likewise, catalysts based on an inverse distribution of the phases, i.e., where the noble metal acts as support and oxide nanoparticles dispersed on the noble metal constitute the active phase, were also used with success in the WGS reaction [24,25]. In any case, the precise active sites for the catalyzed WGS and the corresponding molecular mechanism are not yet completely understood and seem to depend on the catalyst used and on the precise experimental conditions [7,17,26]. This has been elegantly illustrated by Callaghan et al. [27] through a reaction route analysis for the WGS reaction on Cu(1 1 1).

The mechanisms proposed for the WGS on metal-based catalysts can be framed in two general reaction schemes, both starting with water dissociation on the catalysts surface. Next, in the so-called *associative* route, different adsorbed intermediates react whereas in the *redox* route hydroxyl dissociation is involved. An associative mechanism through a carboxyl intermediate was also proposed for the WGS on the Cu(1 1 1) surface on the basis of a careful theoretical study based on periodic density functional calculations [28]. The associative mechanism through a carboxyl intermediary has also been recently proposed for the WGS reaction on Cu and Au nanoparticles dispersed on TiO_2(1 1 0) [7] whereas an associative mechanism through a formate intermediate has also been recently invoked by Águila et al. [29] for the WGS reaction on Cu/ZrO_2 catalysts to explain the observed differences in the activity of the catalysts derived from Cu supported on different

* Corresponding authors. Address: Departament de Química Física & Institut de Química Teòrica i Computacional (IQTCUB), Universitat de Barcelona, C/Martí i Franquès 1, 08028 Barcelona, Spain. Fax: +34 93 402 1231 (F. Illas), +351 234 370 004 (J.R.B. Gomes).
E-mail addresses: francesc.illas@ub.edu (F. Illas), jrgomes@ua.pt (J.R.B. Gomes).

0021-9517/$ - see front matter © 2009 Elsevier Inc. All rights reserved.
doi:10.1016/j.jcat.2009.09.011

ZrO_2 polymorphs. These authors attributed the different activity of the prepared catalysts to the different stability of the formate species on these supports. On the other hand, a redox mechanism at low-temperature has been suggested by Tabatabaei et al. [30] and by Kinch et al. [31] for the WGS reaction on ZnO and Pt/CeO_2(1 1 1) catalysts, respectively. Finally, note that recent density functional calculations indicate that the two pathways compete for the WGS reaction catalyzed by TiC(0 0 1) and that this seems to be indeed a promising catalyst [32].

Relevant information for the molecular mechanism of the WGS reaction catalyzed by Cu and Au nanoparticles has been reported from model density functional calculations [33]. These authors conclude that these systems operate via either redox or associative carboxyl mechanisms and that in each case water dissociation is the rate-limiting step. For the Cu-catalyzed reaction, the recent systematic work of Gokhale et al. [28], combining density functional calculations and a microkinetic analysis, has brought vital additional information concerning the relative importance of the different possible pathways and intermediates in determining the final reaction rate. These authors report a very good agreement between predicted and experimental values for the turnover rate at various conditions even if the theoretical values are obtained using a Cu(1 1 1) surface for modeling of the catalyst. This may seem surprising since low-coordinated atoms are known to be responsible for the catalytic activity in several reactions such as NO dissociation [34,35], CO oxidation [36–38], O_2 dissociation [39], and water decomposition [40]. Therefore, a more detailed exploration of the molecular mechanism of the WGS reaction catalyzed by Cu including the effect of step sites on the calculated energy profiles seems necessary; this is precisely the main goal of the present paper. To this end density functional calculations have been carried out using a Cu(3 2 1)-stepped surface which, due to its *zig-zag* step line, has different low-coordinated atoms and includes a rather high heterogeneity of adsorption sites such as terraces, nearby kinks, and steps and thus, even being obviously less stable than the typical Cu(1 1 1) or Cu(1 0 0) low Miller index surfaces, it provides a way to study the role of more realistic sites as those likely occurring on real catalysts. Using this surface model we consider the most important elementary steps following the reaction scheme of Gokhale et al. [28]. Hence, we first consider direct water splitting into H and OH, which is a common step in the redox and associative mechanisms, and then explore the redox route through hydroxyl disproportionation and the associative route through the carboxyl intermediate with direct carboxyl dehydrogenation or with OH-assisted carboxyl dehydrogenation.

2. Catalyst surface model and computational details

The Cu(3 2 1) surface has been chosen to provide a realistic representation of a Cu catalyst surface containing a variety of surface sites as shown in Fig. 1. Hereafter, the different possible hollow sites are labeled as *a*, *b*, *c*, *d*, *e*, *f*, *g*, *h*, and *i* letters and the top sites as *1*, *2*, *3*, and *4* numbers. The different bridge positions are not illustrated in Fig. 1 but are indicated by the letter *b* followed with the numbers of the two nearest-neighbor copper atoms, ordered with respect to the view from the left to the right and from the positions in the front of the slab (closer to the reader) to those behind (farther to the reader).

The interaction of the different reactants, intermediates, and products involved in the WGS reaction with the Cu(3 2 1) surface was obtained from the periodic density functional calculations modeled through the usual repeated slab approach with the slab constructed using a lattice parameter of 3.638 Å consistent with the computational method chosen here and determined in previous work [41]. The unit cell for the Cu(3 2 1) slab model contains 15 atoms distributed in four atomic layers and consists of a monoclinic prism with the angle between the *x* and *y* axes being different from 90° and the two other involving the *xz* and *yz* axes of exactly 90°. Further, the unit cell vectors along the *x*, *y* and *z* directions have different lengths. The corresponding fractional coordinates of the atoms in this unit cell were obtained using the symmetry features of the CRYSTAL98 computer code [42]. The unit cell for the two-dimensional slab thus constructed was modified by adding a vacuum region of 10 Å and scaling the fractional coordinates to obtain a unit cell that can be replicated in three dimensions as required when using a plane-wave periodic density functional approach (see below). The resulting slab was further modified by allowing full relaxation of the position of the uppermost seven Cu atoms within the computational approach described in more details below. It is worth noting that, following the notation proposed by McFadden et al. [43] for this type of stepped surfaces, the uppermost relaxed surface directly interacting with the adsorbates is the Cu(3 2 1)^S face.

Very recently, we investigated the influence of the exchange-correlation functional in the description of the water adsorption and dissociation on the Cu(1 1 1) surface [41] and found that PBE [44] and PW91 [45] functionals led to the same results while the RevPBE [46] functional led to qualitatively different results, specially for the adsorption of water. Therefore, the periodic density calculations have been carried out using the PW91-generalized gradient approach exchange-correlation potential [45] as implemented in the VASP 4.6.3 computer code [47–49]. The valence electron density has been expanded in a plane-wave basis set with a cutoff of 415 eV for the kinetic energy. The effect of core electrons in the valence electron density has been taken into account through the projector augmented wave (PAW) method [50] as implemented in VASP [51]. Numerical integration in the reciprocal space was carried out by employing a $7 \times 7 \times 1$ Monkhorst–Pack grid of special k-points [52]. The energy cutoff and k-point grid values were chosen after a systematic study of the geometry and energy convergence with the k-points grid and cutoff energy for the water, hydroxyl, and CO adsorptions on the Cu(3 2 1) surface. These test calculations also evidenced that it is not necessary to consider the spin-polarization in the calculations for achieving convergence.

During the geometry optimization calculations carried out to locate the most stable structure of adsorbed species, the positions of the ions were relaxed using the conjugate-gradient algorithm. The transition states for the different elementary steps were determined with the Dimer approach [53]. The convergence criteria were 10^{-6} eV for the total energy and 10^{-3} eV/Å for the forces acting on the ions. These quite strict criteria are necessary in the TS search to avoid the algorithm converging at local minima which are numerous on this stepped surface. A proper frequency analysis indicating the presence of single imaginary frequencies ensured that the structures located with the Dimer method correspond to true transition states. Adsorption energies, co-adsorption energies, and energetic barriers were corrected for the *zero point vibrational energy* (ZPVE correction) using the harmonic oscillator approach and, therefore, the subsequent presentation and discussion of results consider always ZPVE-corrected energies. Uncorrected values are also given in the tables for comparison with the results given in previous works where ZPVE corrections were not taken into account.

Finally, the rate constant (k) at 463 K of each individual reaction step was estimated from the transition state theory [54] as in Eq. (1)

$$k = \left(\frac{k_B T}{h}\right)\left(\frac{q^{\neq}}{q}\right) e^{\frac{-E_a}{k_B T}} \tag{1}$$

where k_B is the Boltzmann constant, T is the absolute temperature, h is the Planck's constant, and E_a is the activation energy from the

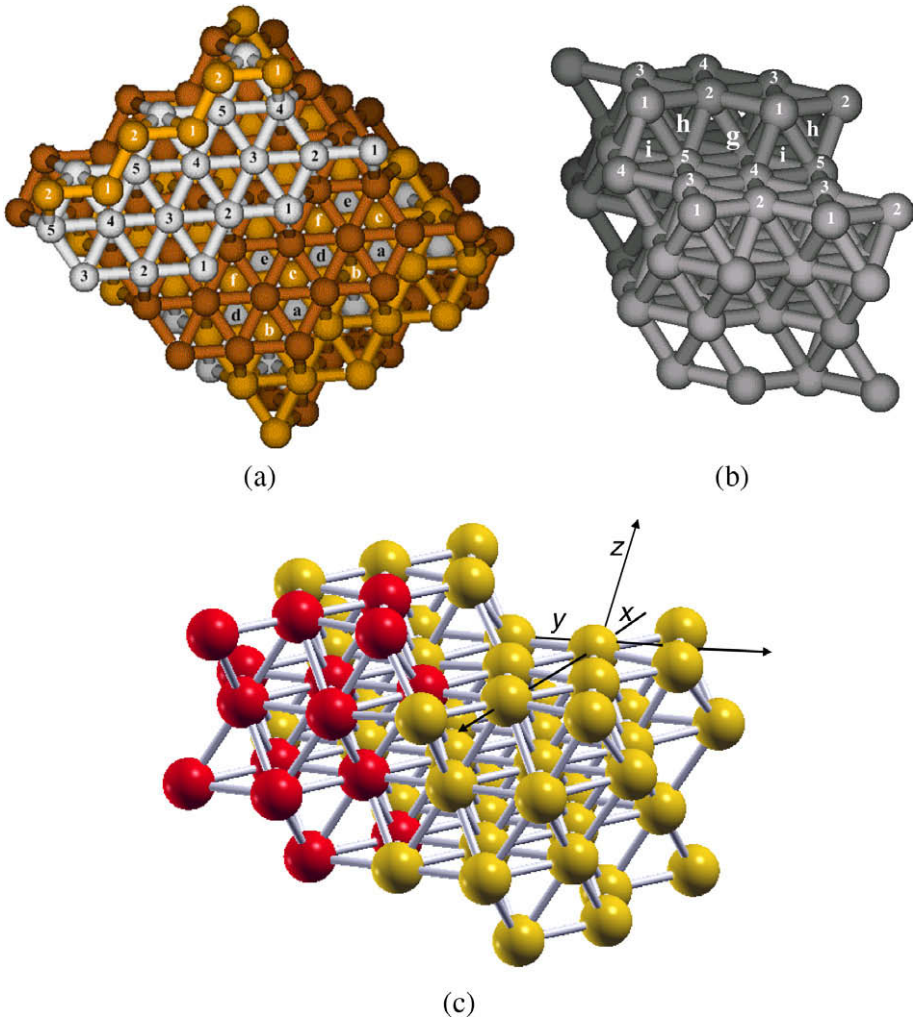

Fig. 1. (a) Top and (b) side views of possible adsorption sites on the Cu(3 2 1) surface. In (c), the fifteen copper atoms of the unit cell and the cell vectors are shown. *a*, *b*, *c*, *d*, *e*, *f*, *g*, *h*, and *i* correspond to hollow positions and *1*, *2*, *3*, *4*, and *5* to the top positions.

ZPVE-corrected calculated energy barrier. Finally, $q^{\neq}$ and q are the partition functions for the TS and initial state, respectively, which have been approximated from the harmonic vibrational frequencies. This procedure provides a good estimate of the rate constant to the point that for the dissociation of N_2 on a stepped Ru(0001) surface the values obtained from this approximated transition state theory are in excellent agreement with converged six-dimensional quantum calculations [55].

3. Reaction mechanisms

Before exposing the results we find it convenient to briefly summarize the most salient features of the reaction mechanisms proposed for the WGS reaction. These can be grouped in two general mechanisms, namely *redox* and *associative*, although with at least two variants in each route. Both mechanisms share the first three elementary steps which correspond to CO and H_2O adsorptions and subsequent H_2O dissociation into adsorbed H and OH as in Eq. (2) below

$$\begin{aligned} &CO + * \rightarrow CO^* \\ &H_2O + * \rightarrow H_2O^* \\ &H_2O^* \rightarrow OH^* + H^* \end{aligned} \tag{2}$$

and also share the H_2 formation step from H^* and products desorption as in Eq. (3)

$$\begin{aligned} &H^* + H^* \rightarrow H_2^* \\ &H_2^* \rightarrow H_2 \uparrow \\ &CO_2^* \rightarrow CO_2 \uparrow \end{aligned} \tag{3}$$

The main differences between the two mechanisms concern the formation of adsorbed CO_2 and the formation of a second H^* in the redox mechanism. The two possible routes along the *redox* mechanism are outlined in Scheme 1. Both involve CO_2 formation by direct reaction between adsorbed CO and O and differ in the way adsorbed O is produced.

On the other hand, the associative mechanism is based on the formation of intermediates, the decomposition of which originates CO_2. Both formate (HCOO) and carboxyl (OCOH) have been postulated as possible intermediates. However, Gokhale et al.'s study [28] has found that the formate isomer, although formed by CO_2 hydrogenation, only acts as a "spectator" species. The two possible routes for the associative mechanism through the carboxyl intermediate can be summarized as in Scheme 2. Both start by the formation of the carboxyl intermediate and differ in the way that this species further evolves.

To investigate these mechanisms for the WGS reaction on the Cu(3 2 1) surface one needs to obtain the configurations of the species in the initial, transition, and final states for each individual reaction step. This requires studying the adsorption or co-adsorption of the different reactants, intermediates, and products on this

Redox mechanism through direct water dissociation

$$OH^* \rightarrow O^* + H^*$$

Redox mechanism through hydroxyl disproportionation

$$OH^* + OH^* \rightarrow O^* + H_2O^*$$

$$CO^* + O^* \rightarrow CO_2^*$$

Scheme 1.

Associative mechanism through carboxyl intermediary with direct dehydrogenation

Associative mechanism through carboxyl intermediary with assisted dehydrogenation

$$CO^* + OH^* \rightarrow OCOH$$

$$OCOH^* \rightarrow CO_2^* + H^*$$

$$OCOH^* + OH^* \rightarrow CO_2^* + H_2O^*$$

Scheme 2.

catalyst surface model and determining the transition state that, for each individual step, connects the most stable configuration of the reactants to the products. The results concerning this analysis are described in the next section.

4. Adsorption state of reactants and products

The most favorable adsorption and co-adsorption configurations of the species entering into the mechanisms of the WGS reaction on the Cu(3 2 1) surface have been obtained by means of geometry optimization. The adsorption energies (E_{ads}) of the isolated species H_2O, CO, OH, H, OCOH, CO_2, and H_2 on the slab surface model were calculated as:

$$E_{ads} = E_{slab-adsorbate} - E_{slab} - E_{adsorbate} \quad (4)$$

where E_{slab} refers to the total energy of the slab model representing the Cu(3 2 1) surface, $E_{adsorbate}$ refers to the total energy of the corresponding adsorbate on the gas phase computed by placing it in a sufficiently large box, and $E_{slab\text{-}adsorbate}$ refers to the total energy of the slab–adsorbate system. For the situations with two adsorbates above the surface unit cell, the adsorption energies ($E_{co\text{-}ads}$) of the co-adsorbed species OH + H, CO + OH, OH + OH, O + H, CO + O, H_2O + O, H + H, CO_2 + H, and CO_2 + H_2O on the slab were calculated as:

$$E_{co-ads} = E_{slab-(frag1+frag2)} - E_{slab} - E_{frag1} - E_{frag2} \quad (5)$$

where E_{slab} is as in Eq. (4), $E_{frag1(frag2)}$ stands for the total energy of the corresponding fragment for the OH + H, CO + OH, OH + OH, O + H, CO + O, H_2O + O, H + H, CO_2 + H, and CO_2 + H_2O pairs in the gas phase; and $E_{slab\text{-}(frag1+frag2)}$ refers to the total energy of the slab-(frag1 + frag2) system. Therefore, negative values of E_{ads} ($E_{co\text{-}ads}$) mean favorable adsorption (co-adsorption). A summary of the results for the most stable adsorption or co-adsorption configuration of each species or a pair of adsorbates is given in Tables 1 and 2, respectively.

According to the present results, water adsorption on the Cu(3 2 1) surface is most favorable in the region of the step with the molecule interacting simultaneously through its oxygen atom with the kink and through one of its hydrogen atoms with the nearest terrace; the adsorption energy for this configuration is −0.58 eV (−0.59 eV, without ZPVE correction). Note that this adsorption energy is about three times larger than the adsorption energy calculated for water on the perfect terrace sites of the Cu(1 1 1) surface [28,41], evidencing the importance of the low-coordinated Cu atoms in the stabilization of the adsorbates. Also the calculated adsorption energy for H_2O on Cu(3 2 1) is larger than the corresponding value on the Au(3 2 1) surface (−0.35 eV) [35], as expected. However, from these data one cannot extract conclusions about the overall catalytic performance of Au-based catalyst for the WGS reaction. In fact, some Au-based catalysts exhibit indeed a high performance for the WGS reaction [5] implying that water adsorption energy does not constitute a reliable descriptor for this reaction and that other factors as the influence of the support are crucial. The CO adsorption on the Cu(3 2 1) surface is most favored on the kinks with an adsorption energy of −0.95 eV (−0.99 eV, without ZPVE correction). Interestingly enough, this result is almost the same as that for CO adsorption on the flat Cu(1 1 1) surface [28], and only slightly more negative than the result for CO adsorption on the analogous Au(3 2 1) surface [38].

On the other hand, the OH and OCOH intermediates are more stable when adsorbed on b_{2-1} sites of the Cu(3 2 1) surface through the O atom and through the HO–CO bond (Fig. 2). The calculated adsorption energies are −3.40 eV (−3.52 eV without ZPVE correction) and −1.95 eV (−2.01 eV without ZPVE correction) for the OH and OCOH intermediates, respectively. The OH radical is clearly more stabilized in the Cu(3 2 1) surface than in the flat Cu(1 1 1) surface [28] and than in the Au(3 2 1) surface where the calculated adsorption energy using the same density functional approach is of −2.42 eV [56]. Further, on the Cu(3 2 1) surface, the adsorption of the carboxyl intermediate is only ∼0.2 eV stronger than that on the Cu(1 1 1) surface [28].

The WGS reaction products, CO_2 and H_2, interact weakly with the Cu(3 2 1) surface with adsorption energies of −0.06 eV and −0.12 eV (−0.07 eV and −0.13 eV without ZPVE correction), respectively. The CO_2 adsorption energy is almost the same as that for its adsorption on the flat Cu(1 1 1) surface [28] as expected from the difficulty to activate CO_2 even on more reactive transition metal surfaces [57]. Interestingly, the H_2 molecule adsorbs on the Cu(3 2 1) surface while it does not adsorb on the flat Cu(1 1 1) surface [28]. Co-adsorptions of OH + H, CO + OH, OH + OH, O + H, CO + O, H_2O + O, H + H, CO_2 + H, and CO_2 + H_2O pairs on the Cu(3 2 1) slab have also been considered since these are necessary in order to obtain the energy profile for each individual step. A schematic representation of the most stable configuration for each situation (adsorption or co-adsorption) is shown in Fig. 2.

The results of this section can be simply summarized by stating that the presence of surface steps has an important effect in the adsorption of some reactants and products such as H_2O, H_2 molecule, and the OH radical, but it has a weakly effect in the adsorption of other species such as CO, CO_2, and carboxyl. The effect of these differences in the resulting energy profile for each mechanism is discussed in the next section.

Table 1
Adsorption energies (E_{ads}, eV) and structural parameters (d, Å) for the adsorption of the WGS reaction species on Cu(321).[a]

Species	Adsorption site	E^{e}_{ads}	E^{o}_{ads}	Vibrational modes[b]	$d_{suf-mol}$[c]	Bond length[d]
H_2O	top1-step	−0.59	−0.58	3708, 3426, 1557	O-(*1*): 2.14	0.98 ($O–H_a$) 0.99 ($O–H_b$)
OH	b_{2-1}	−3.52	−3.40	3718, 648, 531	O-(*1*): 1.95 O-(*2*): 1.98	0.97 (O–H)
CO	top1	−0.99	−0.95	2065	C-(*1*): 1.84	1.15 (C–O)
OCOH	b_{2-1}	−2.01	−1.95	3335, 1667, 1097 889, 670, 539	C-(*1*): 1.95 O_b-(*2*): 2.15	1.22 ($C–O_a$) 1.41 ($C–O_b$) 1.00 (O_b–H)
CO_2	b_{1-3}	−0.07	−0.06	2354, 1321, 618 603	O_a-(*1*): 2.89 O_b-(*3*): 3.95	1.18 ($C–O_{a,b}$)
H_2	top1	−0.13	−0.12	3679, 949, 546	$H_{a,b}$-(*1*): 1.81	0.79 (H–H)

[a] In (E_{ads}), the "e" and "o" labels stand for uncorrected and ZPE-corrected values.
[b] Only the vibrational modes above 500 cm^{-1} are shown.
[c] Distances between the adsorbate's nearest atoms to the Cu(321) surface; the label of the Cu surface atom is indicated between parenthesis.
[d] Adsorbate's internal lengths involving the atoms indicated between parenthesis.

Table 2
Co-adsorption energies ($E_{co\text{-}ads}$, eV) and structural parameters (d, Å) for the co-adsorption of the WGS reaction species on Cu(321).[a]

Species	Adsorption site	E^{e}_{co-ads}	E^{o}_{co-ads}	Vibrational modes[b]	$d_{suf-mol}$[c]	Bond length[d]
OH + H	b_{4-1}/hole "a"	−5.73	−5.47	3659, 1286, 956 745, 659, 519	O-(*1*): 1.95 O-(*4*): 1.95 H-(*1*): 1.63 H-(*2*): 1.76 H-(*3*): 1.78	0.97 (O–H)
CO + OH	top1/hole "a"	−4.20	−4.05	3721, 2010, 580 545	C-(*1*): 1.84 O-(*1*): 1.98 O-(*2*): 2.06 O-(*3*): 2.06	0.97 (O–H) 1.16 (C–O)
OH + OH	b_{2-1}/b_{3-1}	−6.64	−6.40	3697, 3574, 794 669, 638, 545	O_a-(*1*): 1.99 O_a-(*2*): 1.95 O_b-(*1*): 2.02 O_b-(*3*): 2.00	0.98 ($O_a–H_a$) 0.98 ($O_b–H_b$)
O + H	hole "a"/b_{4-1}	−7.56	−7.31	1519, 1249	H-(*1*): 1.57 H-(*2*): 1.65 O-(*1*): 1.84 O-(*2*): 1.89 O-(*3*): 1.92	
CO + O	top1/hole "a"	−5.95	−5.84	2081	C-(*1*): 1.84 O-(*1*): 1.92 O-(*2*): 1.88 O-(*3*): 1.90	1.15 (C–O)
H_2O + O	top1-step/hole "b"	−5.85	−5.67	3741, 2685, 1603 950, 654	O_{H_2O}-(1): 2.07 O-(*1*): 2.01 O-(*2*): 1.91 O-(*3*): 1.95	0.97 ($O–H_a$) 1.03 ($O–H_b$)
H + H	hole "f"/hole "a"	−6.11	−5.81	1144, 957, 923 877, 745	H_a-(*1*): 1.70 H_a-(*2*): 1.75 H_a-(*3*): 1.79 H_b-(*1*): 1.76 H_b-(*3*): 1.86 H_b-(*4*): 1.75 H_b-(*5*): 1.96	
CO_2 + H	terrace/hole "b"	−2.64	−2.47	2347, 1321, 1127 862, 696, 628, 609	H-(*1*): 1.71 H-(*2*): 1.75 H-(*3*): 1.80	1.18 ($C–O_a$) 1.18 ($C–O_b$)
CO_2 + H_2O	terrace/top1-step	−0.71	−0.70	3704, 3444, 2348 1562, 1318, 621 613, 536	O_{H_2O}-(1): 2.14 O_a-(*1*): 5.11 O_b-(*2*): 4.84	0.98 ($O–H_a$) 0.99 ($O–H_b$) 1.18 ($C–O_a$) 1.18 ($C–O_b$)

[a] In the adsorption (E_{ads}) and co-adsorption ($E_{co\text{-}ads}$), the "e" and "o" labels stand for uncorrected and ZPE-corrected values.
[b] Only the vibrational modes above 500 cm^{-1} are shown.
[c] Distances between the adsorbate's nearest atoms to the Cu(321) surface; the label of the Cu surface atom is indicated between parenthesis.
[d] Adsorbate's internal lengths involving the atoms indicated between parenthesis.

5. Activation energy barriers and rate constants

In this section we focus on the calculated activation energies and estimated rate constants which are the core of the present work. The activation energy barrier for each individual step of the reaction mechanism discussed above has been calculated as the energy difference between the transition state, located using the Dimer method [53], and that of the most stable adsorption (or co-adsorption) configuration for the reactant(s) is taken as the initial state. Due to the special features of the energy profile

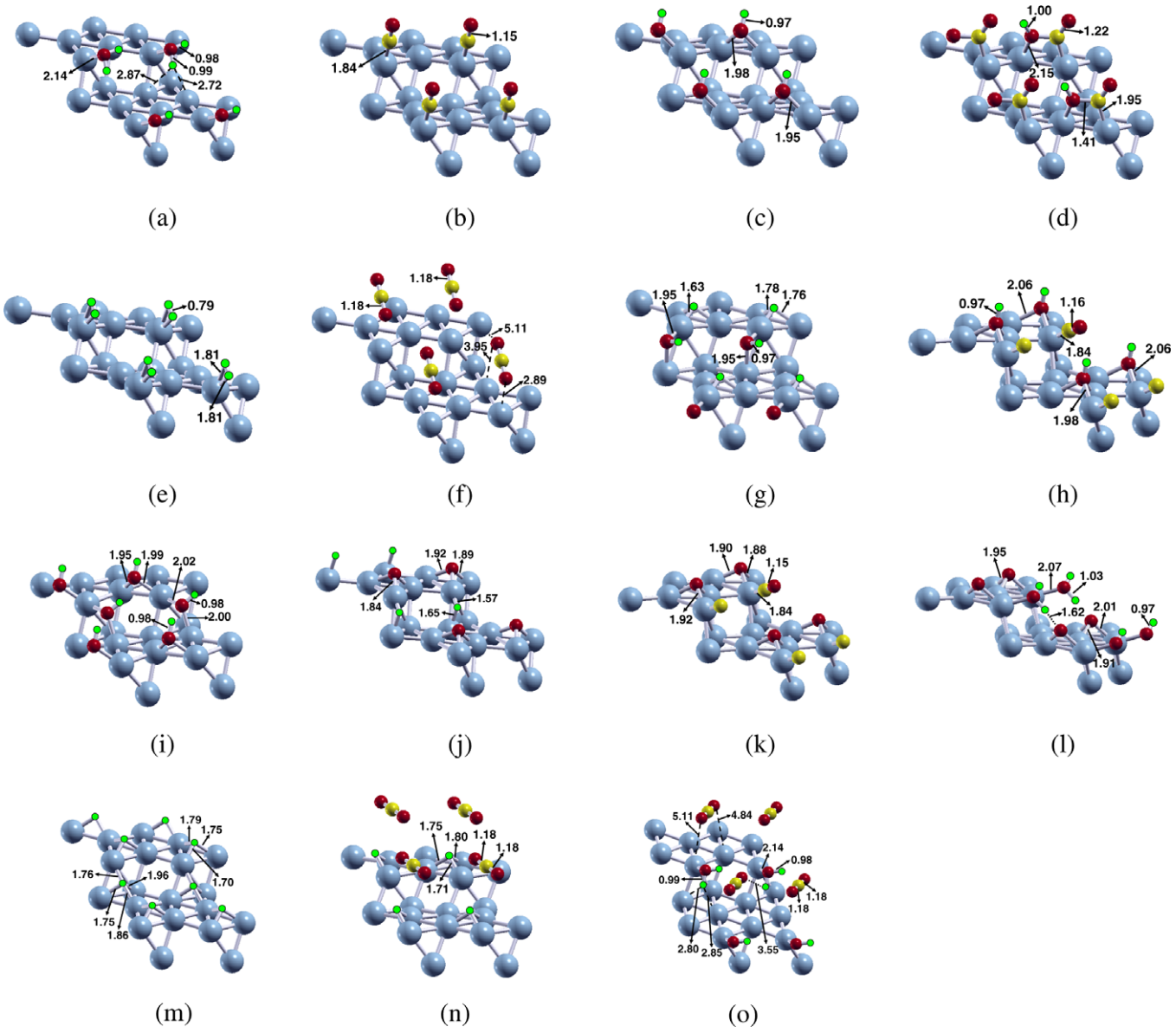

Fig. 2. Most stable configuration for the (a) H_2O, (b) CO, (c) OH, (d) OCOH, (e) H_2, (f) CO_2, (g) OH + H, (h) CO + OH, (i) OH + OH, (j) O + H, (k) CO + O, (l) H_2O + O, (m) H + H, (n) CO_2 + H, and (o) CO_2 + H_2O adsorbed (co-adsorbed) on the Cu(3 2 1) surface. Only the outermost copper layer is shown. Red is used for oxygen, yellow for carbon, green for hydrogen, and blue for copper. All distances are given in Å. (For interpretation of the references to colour in this figure legend, the reader is referred to the web version of this article.)

for desorption pathways ($H_2^* \rightarrow H_2\uparrow$ and $CO_2^* \rightarrow CO_2\uparrow$), the TS states were assumed to be close to those of the products. Further, the energy barriers thus obtained were corrected with the ZPVE. Uncorrected and corrected values are given in Table 3, together with the reaction energies and reaction rate constants of each individual step. The rate constants were calculated for a temperature of 463 K, a typical value for the low-temperature water gas shift reaction [58]. Schematic representations of the transition states are given in Fig. 3 whereas a comparison of the reaction profiles for the different routes is made in Fig. 4.

Analyzing the activation energy barrier and rate constants obtained for the WGS reaction on the Cu(3 2 1) surface modeling a catalyst surface exposing low-coordinated sites, we can see that the initial step, $H_2O^* \rightarrow OH^* + H^*$ common to the redox and associative mechanisms, is limited by an activation energy barrier of 0.71 eV (0.93 eV without ZPVE correction). As expected from previous works, the presence of step sites has a strong influence on the activation energy [59–61]. For this particular elementary reaction, the activation energy barrier calculated for the Cu(3 2 1) surface is significantly lower than the activation energy barrier obtained for the same reaction step in the flat Cu(1 1 1) surface, i.e. 0.92 [41] or 1.36 eV [28] without the ZPVE correction. On the other hand, our value is close to that reported for the Cu(1 1 0) surface which presents low coordinated Cu [62–65]. Thus, the present results provide further evidence of the surface structure sensitivity of this reaction and of the importance of the low-coordinated Cu atoms. For water dissociation, the comparison to the analogous Au(3 2 1) surface, where the activation energy barrier is 1.33 eV [66], clearly evidences that this step is easier on the Cu(3 2 1) surface. On the other hand, one must realize that this value of the energy barrier is considerably higher than the one obtained for the same reaction on oxide surfaces [67], thus supporting the idea that the oxide plays a decisive role in the performance of copper/oxide WGS catalysts [68]. On the other hand, the presence of steps has almost no

Table 3
Activation energies (E_a, eV), vibrational modes (cm^{-1}), bond length for the TS (Å), reaction rate constants at 463 K (k, s^{-1} or $mol^{-1}\,s^{-1}$), reaction energy (Δ), and imaginary frequencies (cm^{-1}) for the different steps of the WGS reaction on the Cu(321) surface.[a]

Elementary step	Vibrational modes[b]	Bond length[c]	E_a^e	E_a^o	k	Δ_e	Δ_o	Imaginary frequency
$H_2O^* \rightarrow OH^* + H^*$	3679, 784, 673, 583	1.63	0.93	0.71	3.6×10^4	0.33	0.22	820
$OH^* \rightarrow O^* + H^*$	986, 607, 526	1.58	1.74	1.55	4.1×10^{-5}	0.72	0.64	537
$OH^* + OH^* \rightarrow O^* + H_2O^*$	3715, 2975, 1572, 876, 530	1.84	0.79	0.78	1.47×10^4	0.08	0.09	149
$CO^* + O^* \rightarrow CO_2^*$	2081	1.80	0.62	0.60	5.58×10^5	−0.55	−0.49	307
$CO^* + OH^* \rightarrow OCOH^*$	3721, 2010, 580, 545	1.78	0.47	0.46	2.33×10^7	0.18	0.22	244
$OCOH^* \rightarrow CO_2^* + H^*$	1747, 1160, 845, 662, 556	1.44	1.32	1.10	9.67×10^1	−0.28	−0.39	1459
$OCOH^* + OH^* \rightarrow CO_2^* + H_2O^*$	3660, 2223, 1745, 1171, 778, 737, 718, 547	1.51	0.65	0.55	9.72×10^6	−0.74	−0.72	468
$H^* + H^* \rightarrow H_2^*$	1466, 1286, 514	1.04	0.87	0.80	3.91×10^4	0.31	0.35	772
$H_2^* \rightarrow H_2\uparrow$	–	–	0.13	0.12	3.45×10^{11}	0.13	0.12	–
$CO_2^* \rightarrow CO_2\uparrow$	–	–	0.07	0.06	4.49×10^{11}	0.07	0.06	–

[a] In the activation (E_a) and reaction energies (Δ), the "e" and "o" labels stand for uncorrected and ZPVE-corrected values.
[b] Only the vibrational modes above 500 cm^{-1} are shown.
[c] Length of the bond breaking (or forming) in the transition state.

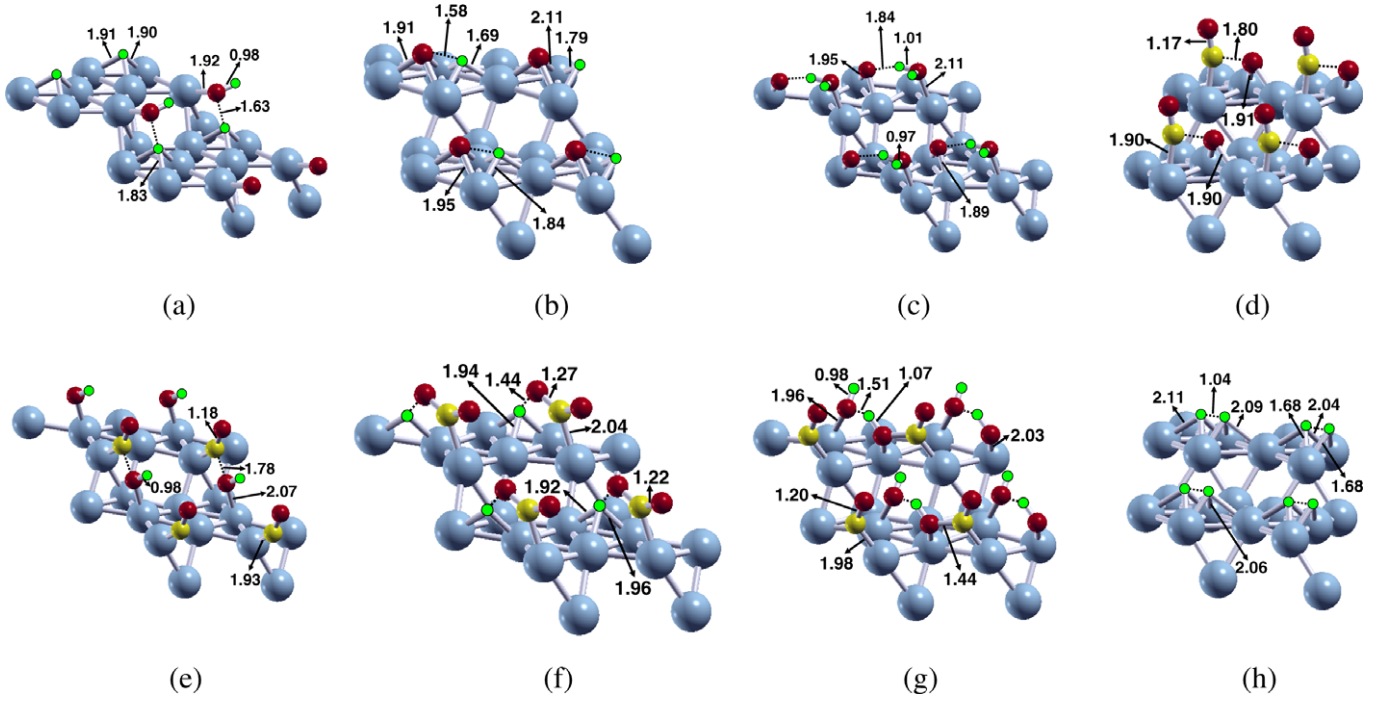

Fig. 3. Transition state configuration for the (a) $H_2O^* \rightarrow OH^* + H^*$, (b) $OH^* \rightarrow O^* + H^*$, (c) $OH^* + OH^* \rightarrow O^* + H_2O^*$, (d) $CO^* + O^* \rightarrow CO_2^*$, (e) $CO^* + OH^* \rightarrow OCOH^*$, (f) $OCOH^* \rightarrow CO_2^* + H^*$, (g) $OCOH^* + OH^* \rightarrow CO_2^* + H_2O^*$, and (h) $H^* + H^* \rightarrow H_2^*$ reaction on the Cu(321) surface. Red is used for O, yellow for C, green for H, and blue for Cu. All the distances are given in Å. (For interpretation of the references to colour in this figure legend, the reader is referred to the web version of this article.)

effect on the reaction energy (Δ in Table 3) for this step. The calculated value of 0.22 eV (0.33 eV without ZPVE correction) coincides with the value reported for water dissociation on the flat Cu(111) surface [41] although still ~0.3 eV larger than the value reported by Gokhale et al. for the same surface [28]; this discrepancy is probably due to the differences in the calculation parameters. The reaction rate constant for this step has an estimated value of $3.62 \times 10^4\ s^{-1}$ at 190 °C (463 K) suggesting that this, together with the hydrogen recombination ($k = 3.91 \times 10^4\ mol^{-1}\,s^{-1}$), is the rate-limiting step for the WGS reaction on the Cu(321) surface. Further, this reaction rate constant is three order of magnitude larger than the value estimated for the water dissociation on the flat Cu(111) surface [41].

After the initial water dissociation step, there are three possibilities to continue the WGS process as explained in detail in a previous section. Thus, OH^* obtained in the water dissociation can be further dissociated to provide $O^* + H^*$ (redox mechanism with direct OH^* dissociation), react with another OH^* (redox mechanism with OH^* disproportionation), or react with the CO^* to produce $OCOH^*$ (associative mechanism through the carboxyl intermediary). According to the present results (Fig. 4), the WGS reaction will proceed through the OCOH intermediate. The preference for the associative mechanism is in agreement with the results obtained for the WGS reaction on the Cu(111) surface [28]. Thus, even if the presence of steps will certainly accelerate the reaction, the main conclusions obtained by means of a Cu(111) surface model of the catalyst remain valid.

The formation of the $OCOH^*$ carboxyl radical faces an activation energy barrier of 0.46 eV (0.47 eV without ZPVE correction) while the direct OH^* dissociation and the OH^* disproportionation are limited by activation energy barriers of 1.55 eV (1.74 eV without ZPVE correction) and 0.78 eV (0.79 eV without ZPVE correction), respectively. The calculated reaction rate constants also confirm the preference for the route through the $OCOH^*$ intermediate since the rate constant for $OCOH^*$ formation is $2.33 \times 10^7\ mol^{-1}\,s^{-1}$, whereas values of $4.07 \times 10^{-5}\ s^{-1}$ and $1.47 \times 10^4\ mol^{-1}\,s^{-1}$ are obtained for

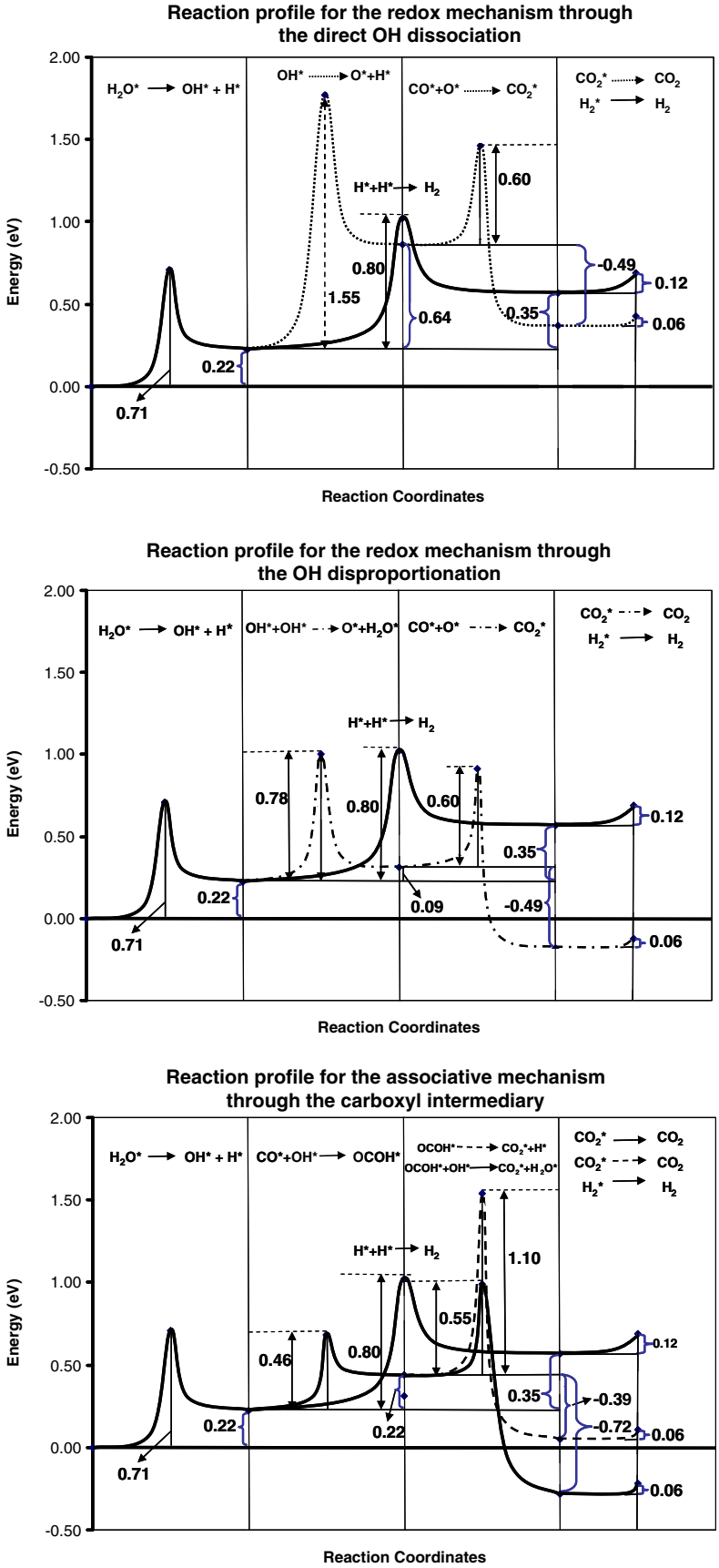

Fig. 4. Global reaction profiles for the possible mechanisms of the WGS reaction on the Cu(321) surface: direct redox mechanism (top panel), OH-assisted redox mechanism (medium panel), and associative mechanism (bottom panel). Straight line represents the most favorable reaction steps for $CO_2 + H_2$ formation. All energies are given in eV.

OH^* dissociation and OH^* disproportionation, respectively. Interestingly, the activation energy barrier for OH^* direct dissociation on the Cu(3 2 1) surface coincides with the value obtained for this elementary step on the flat Cu(1 1 1) surface [28] while the activation energy barrier for the OH^* disproportionation is considerably higher on the Cu(3 2 1) surface. The latter is due to the strong stabilization of the co-adsorbed $OH^* + OH^*$ on the Cu(3 2 1) surface, which hinders the diffusion needed to reach the dissociation conformation.

Although the present results clearly show that the redox mechanism through either direct OH^* dissociation or OH^* disproportionation is unfavorable, we find it convenient to discuss the subsequent steps for these routes. Direct CO^* oxidation by O^* requires an activation energy barrier of 0.60 eV (0.62 eV without ZPVE correction) and results in a reaction energy of −0.49 eV (−0.55 eV without ZPVE correction). This activation energy barrier is ~0.2 eV lower than the value obtained for the reaction on the Cu(1 1 1) surface once again confirming the importance of the step sites as active sites for catalytic reactions. However, it is worth mentioning that the same reaction has an almost null barrier on the analogous Au(3 2 1) surface [38]. On the Cu(3 2 1) surface, the reaction rate constant for this step is 5.58×10^5 mol^{-1} s^{-1} corresponding to a rather fast reaction although this step is hindered by the previous steps on this route. The steps following CO^* oxidation by O^* in the redox mechanism are common to the associative mechanism and will be discussed later.

Let us now consider the steps in the associative mechanism following $OCOH^*$ formation. Two possibilities exist for the carboxyl dehydrogenation, namely the direct OCO–H bond breaking on the metallic surface and the OCO–H bond breaking assisted by an OH^*. For the direct dehydrogenation a rather large activation energy barrier of 1.10 eV (1.32 eV without ZPVE correction) is found which results in a small reaction rate constant of 9.67×10^1 s^{-1} and in reaction energy of −0.39 eV (−0.28 eV without ZPVE correction). Consequently, this reaction step is very unlikely. On the other hand, the carboxyl dehydrogenation assisted by an OH^* has considerably lower activation energy barrier of 0.55 eV (0.64 eV without ZPVE correction) only. The corresponding reaction rate constant for this step is considerably larger (9.72×10^6 mol^{-1} s^{-1}) with a considerable exothermicity of −0.72 eV (−0.74 eV without ZPVE correction). The activation energy barrier for the carboxyl dehydrogenation assisted by an OH^* is only slightly higher than the activation energy barrier calculated for the same reaction on the flat Cu(1 1 1) surface [28], probably due again to the strong stabilization of the co-adsorbed reagents on the Cu(3 2 1) surface which increases the diffusion energy necessary to achieve the structure required for the reaction.

The hydrogen recombination is a step common to the four investigated routes and according to the present results, the H^* atoms are only provided by water dissociation because the two other possible steps generating H^* (OH^* dissociation and direct carboxyl dehydrogenation) are very unfavorable even in this stepped Cu(3 2 1) surface. Hydrogen recombination requires an activation energy barrier of 0.80 eV (0.87 eV without ZPVE correction), which leads to a reaction rate constant of 3.91×10^4 mol^{-1} s^{-1}. This means that this step, together with water dissociation into OH^* and H^*, is one of the rate-limiting steps for the WGS on this surface. Moreover, the hydrogen recombination is endothermic by 0.35 eV (0.31 eV without ZPVE correction). Nevertheless, both, the activation energy barrier and reaction energy values, are lower than those corresponding to the same elementary step on Cu(1 1 1) [28], thus indicating that the process will be easier on the Cu(3 2 1) surface than on the flat Cu(1 1 1) surface. On the other hand, on Cu(1 1 1) the water dissociation step has a considerable higher activation energy barrier than the hydrogen recombination [28] whereas on Cu(3 2 1) the two activation energy barriers are more similar, which leads to similar reaction rate constants.

The final steps for the WGS are the CO_2 and H_2 desorptions which in this surface are both very likely since the activation energy barriers (estimated from the desorption energies) are of 0.06 eV (0.07 eV without ZPVE correction) and 0.12 eV (0.13 eV without ZPVE correction) only. These low activation energy barriers for desorption results in rather large rate constants, 4.49×10^{11} s^{-1} and 3.45×10^{11} s^{-1} for CO_2 and H_2 desorptions, respectively, indicating that the reaction products will rapidly leave the surface. Further, the CO_2 desorption energy is the same

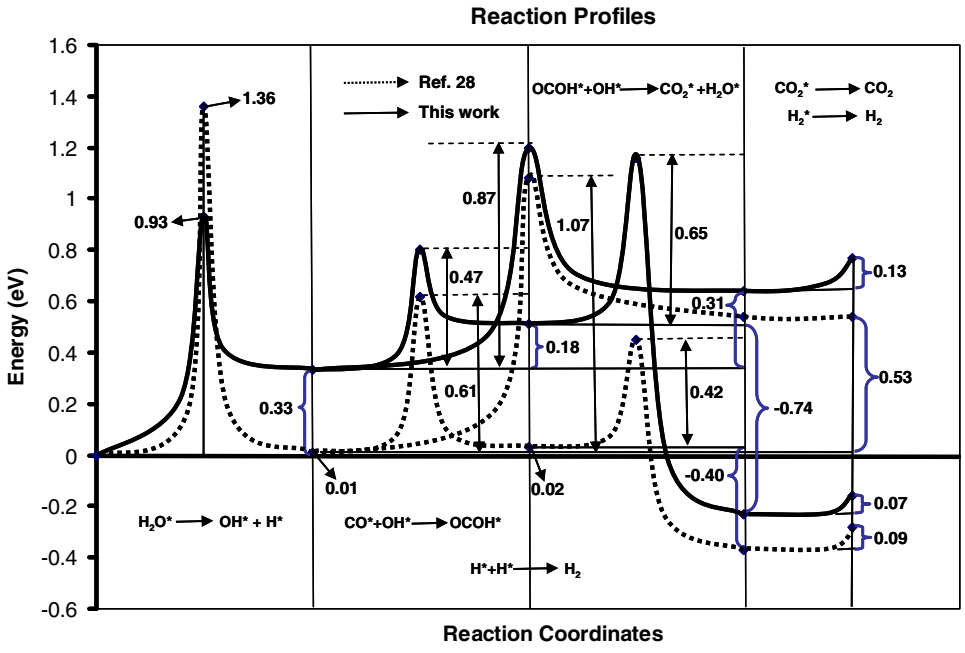

Fig. 5. Comparison of the reaction profiles for the WGS reaction on the flat Cu(1 1 1) surface (data from Ref. [28]) and on the stepped Cu(3 2 1) surface (data from this work). All the energies are given in eV and without ZPVE correction. Note that data for hydrogen desorption step correspond only to the present work.

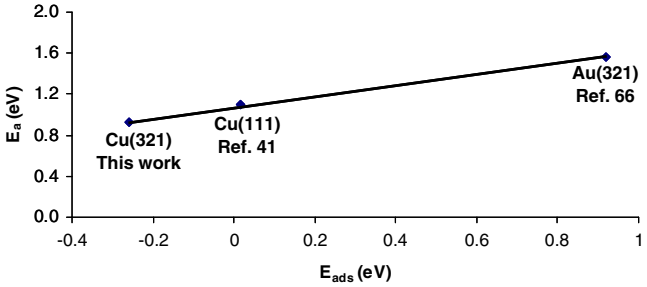

Fig. 6. Representation of the activation energy (E_a) with respect to the adsorption energy (E_{ads}) of the reaction products (given with respect to the gaseous water and the clean slab) for the water dissociation on the flat Cu(1 1 1) surface (data from Ref. [41]), on the Cu(3 2 1) surface (data from this work), and on the Au(3 2 1) surface (data from Ref. [66]). All the energies are given in eV and without ZPVE correction.

as that for the Cu(1 1 1) surface while the H_2 does not adsorb on the Cu(1 1 1) surface [28]. On the other hand, it is illustrative to compare the most favorable reaction pathway for the WGS reaction on Cu(3 2 1) and Cu(1 1 1). Fig. 5 presents the two energy profiles using the data from Gokhale et al. [28] and from the present study. The presence of steps no doubt favors the reaction, enhances the catalytic activity, and largely increases the reaction rate constants. Therefore, the reaction will proceed through the step sites and the terraces will just act as reservoirs. However, it is interesting to see that the preferred mechanism predicted from the two surfaces is the same.

Finally, combining the activation energy (E_a) for the water first proton abstraction and the adsorption energy (E_{ads}) for the reaction products obtained in the present work with previous results obtained for the same reaction on Cu(1 1 1) [41] and Au(3 2 1) [66] using a similar computational procedure it is possible to derive a Brønsted–Evans–Polanyi (BEP) relationship similar to that reported by Nørskov et al. for several elementary steps [69]. For Cu(1 1 1) we used the data from Ref. [41] and not from Ref. [28] just for computational consistency and, on the other hand, the adsorption energies of the reaction products were calculated with respect to gas phase water and the clean slab corresponding to each surface. The BEP relationship in Fig. 6 shows an almost perfect linear correlation between the E_a and the E_{ads} for the different surfaces decreasing the E_a with increasing E_{ads} of the reaction products with $E_a = 0.529\ E_{ads} + 1.077$ and $R^2 = 0.998$. This result can be used to obtain the approximate activation energy barriers on other surfaces from the adsorption energies of the reaction products only.

6. Conclusions

The effect of the surface steps in the mechanism of the water gas shift reaction catalyzed by Cu surfaces has been studied by means of periodic density functional calculations using the stepped Cu(3 2 1) surface as a realistic model of the catalyst surface. Two different mechanisms and two routes per mechanism have been investigated and the structure of reactants, transition states, and products were determined and characterized by proper frequency analysis. From the calculated activation energy barriers and reaction rate constants for the complete set of different elementary steps in these mechanisms it has been concluded that the reaction will proceed following the associative mechanism through the carboxyl intermediate with carboxyl dehydrogenation assisted by adsorbed OH.

It is worth pointing out that the same conclusion has been reached using a flat surface model such as the Cu(1 1 1) surface which does not contain low-coordinated Cu atoms. However, even both surfaces predict the same mechanism and most favorable route, there are important differences between the reaction mechanisms on the two surfaces. The presence of steps increases the water adsorption energy and decreases the activation energy barriers for the rate-limiting steps, which are the dissociation of water into H^* and OH^* and the recombination of hydrogen on the stepped surface. These two reaction steps are also the rate-determining steps for the WGS reaction on Cu(1 1 1) but, on Cu(3 2 1) they have similar activation energy barriers and reaction rate constants, while on the flat Cu(1 1 1) surface the water dissociation has an activation energy barrier considerably larger than the hydrogen recombination.

Comparison with the previous data obtained for the water dissociation elementary step on Cu(1 1 1) and Au(3 2 1) using the same computational approach allowed us to unravel the existence of a Brønsted–Evans–Polanyi linear relationship between the activation energy and the adsorption energy of the products $-OH^* + H^*$ – with respect to the gas phase water molecule and the clean surface. This relationship may then be used in subsequent work to predict the activation energy for this step on other metallic surfaces from the adsorption energies only.

To summarize, the presence of steps on Cu surfaces largely affects the catalytic performance of these systems toward the WGS reaction mainly by decreasing the activation energy barriers for the rate-limiting steps (water dissociation and hydrogen recombination) relative to the values predicted for perfect Cu(1 1 1) terraces. However, the prediction of the preferred associative mechanism for the WGS reaction arising from density functional calculations on a perfectly flat Cu(1 1 1) surface model remains a valid conclusion [28].

Acknowledgments

Financial support from FEDER, Portuguese Fundação para a Ciência e Tecnologia (FCT), Conselho de Reitores das Universidades Portuguesas (CRUP), and Spanish Ministerio de Ciencia e Innovacion (MICCIN) through Grants Programa Ciência 2007, Acção E-43/08, FIS2008-02238, and HP2007-0042 is fully acknowledged. JLCF thanks FCT for a post-doctoral grant (Ref. SFRH/BPD/27167/2006).

References

[1] J.J. Spivey, Catal. Today 100 (2005) 171.
[2] D.J. Suh, C. Kwak, J.-H. Kim, S.M. Kwon, T.-J. Park, J. Power Sources 142 (2005) 70.
[3] D.S. Newsome, Catal. Rev. Sci. Eng. 21 (1980) 275.
[4] N. Schumacher, A. Boisen, S. Dahl, A.A. Gokhale, S. Kandoi, L.C. Grabow, J.A. Dumesic, M. Mavrikakis, I. Chorkendorff, J. Catal. 229 (2005) 265.
[5] R. Burch, Phys. Chem. Chem. Phys. 8 (2006) 5483.
[6] D. Mendes, H. Garcia, V.B. Silva, A. Mendes, L.M. Madeira, Ind. Eng. Chem. Res. 48 (2009) 430.
[7] J.A. Rodríguez, J. Evans, J. Graciani, J.-B. Park, P. Liu, J. Hrbek, J. Fdez. Sanz, J. Phys. Chem. C 113 (2009) 7364.
[8] S.H.D. Lee, D.V. Applegate, S. Ahmed, S.G. Calderone, T.L. Harvey, Int. J. Hydrogen Energy 30 (2005) 829.
[9] A.Y. Rozovskii, G.I. Lin, Top. Catal. 22 (2003) 137.
[10] M.A. LarrubiaVargas, G. Busca, U. Costantino, F. Marmottini, T. Montanari, P. Patrono, F. Pinzari, G. Ramis, J. Mol. Catal. A: Chem. 266 (2007) 188.
[11] L. Li, Y. Zhan, Q. Zheng, Y. Zheng, X. Lin, D. Li, J. Zhu, Catal. Lett. 118 (2007) 91.
[12] F. Boccuzzi, A. Chiorino, M. Manzoli, D. Andreeva, T. Tabakova, J. Catal. 188 (1999) 176.
[13] Z.-P. Liu, S.J. Jenkins, D.A. King, Phys. Rev. Lett. 94 (2005) 196102.
[14] H. Yahiro, K. Murawaki, K. Saiki, T. Yamamoto, H. Yamaura, Catal. Today 126 (2007) 436.
[15] J.A. Rodríguez, P. Liua, J. Hrbek, M. Pérez, J. Evans, J. Mol. Catal. A: Chem. 281 (2008) 59.
[16] P. Kumar, R. Idem, Energy Fuels 21 (2007) 522.
[17] J.A. Rodriguez, P. Liu, X. Wang, W. Wen, J. Hanson, J. Hrbek, M. Pérez, J. Evans, Catal. Today 143 (2009) 45.
[18] X. Wang, J.A. Rodriguez, J.C. Hanson, D. Gamarra, A. Martínez-Arias, M. Fernández-García, J. Phys. Chem. B 110 (2006) 428.
[19] Y. Chen, J. Cheng, P. Hua, H. Wang, Surf. Sci. 602 (2008) 2828.
[20] L. Zhang, X. Wang, J.-M.M. Millet, P.H. Matter, U.S. Ozkan, Appl. Catal. A: Gen. 351 (2008) 1.

[21] X. Du, Z. Yuana, L. Cao, C. Zhanga, S. Wanga, Fuel Process. Technol. 89 (2008) 131.
[22] K. Nishida, I. Atake, D. Li, T. Shishido, Y. Oumi, T. Sano, K. Takehira, Appl. Catal. A: Gen. 337 (2008) 48.
[23] J. Knudsen, A.U. Nilekar, R.T. Vang, J. Schnadt, E.L. Kunkes, J.A. Dumesic, M. Mavrikakis, F. Besenbacher, J. Am. Chem. Soc. 129 (2007) 6485.
[24] X. Zhao, S. Ma, J. Hrbek, J.A. Rodriguez, Surf. Sci. 601 (2007) 2445.
[25] J.A. Rodriguez, S. Ma, P. Liu, J. Hrbek, J. Evans, M. Pérez, Science 318 (2007) 1757.
[26] Y. Li, Q. Fu, M. Flytzani-Stephanopoulos, Appl. Catal. B 27 (2000) 179.
[27] C.A. Callaghan, S.A. Vilekar, I. Fishtik, R. Datta, Appl. Catal. A: Gen. 345 (2008) 213.
[28] A.A. Gokhale, J.A. Dumesic, M. Mavrikakis, J. Am. Chem. Soc. 130 (2008) 1402.
[29] G. Águila, S. Guerrero, P. Araya, Catal. Commun. 9 (2008) 2550.
[30] J. Tabatabaei, B.H. Sakakini, K.C. Waugh, Catal. Lett. 110 (2006) 77.
[31] R.T. Kinch, C.R. Cabrera, Y. Ishikawa, J. Phys. Chem. C 113 (2009) 9239.
[32] F. Viñes, J.A. Rodriguez, P. Liu, F. Illas, J. Catal. 260 (2008) 103.
[33] P. Liu, J.A. Rodriguez, J. Chem. Phys. 126 (2007) 164705.
[34] C.P. Vinod, J.W.N. Hansa, B.E. Nieuwenhuys, Appl. Catal. A: Gen. 291 (2005) 93.
[35] J.L.C. Fajín, M.N.D.S. Cordeiro, J.R.B. Gomes, J. Phys. Chem. C 113 (2009) 8864.
[36] N. Lopez, T.V.W. Janssens, B.S. Clausen, Y. Xu, M. Mavrikakis, T. Bligaard, J.K. Nørskov, J. Catal. 223 (2004) 232.
[37] I.N. Remediakis, N. López, J.K. Nørskov, Appl. Catal. A: General 291 (2005) 13.
[38] J.L.C. Fajín, M.N.D.S. Cordeiro, J.R.B. Gomes, J. Phys. Chem. C 112 (2008) 17291.
[39] J.L.C. Fajín, M.N.D.S. Cordeiro, J.R.B. Gomes, J. Phys. Chem. C 111 (2007) 17311.
[40] M.A. Henderson, Langmuir 12 (1996) 5093.
[41] J.L.C. Fajín, F. Illas, J.R.B. Gomes, J. Chem. Phys. 130 (2009) 224702.
[42] V.R. Saunders, R. Dovesi, C. Roetti, M. Causà, N.M. Harrison, R. Orlando, C.M. Zicovich-Wilson, Computer Code CRYSTAL 98, User's Manual (University of Torino), Torino, 1998.
[43] C.F. McFadden, P.S. Cremer, A.J. Gellman, Langmuir 12 (1996) 2483.
[44] J.P. Perdew, K. Burke, M. Ernzerhof, Phys. Rev. Lett. 67 (1996) 3865.
[45] J.P. Perdew, J.A. Chevary, S.H. Vosko, K.A. Jackson, M.R. Pederson, D.J. Singh, C. Fiolhais, Phys. Rev. B 46 (1992) 6671.
[46] Y. Zhang, W. Yang, Phys. Rev. Lett. 80 (1998) 890.
[47] G. Kresse, J. Hafner, Phys. Rev. B 47 (1993) 558.
[48] G. Kresse, J. Furthmüller, Comput. Mater. Sci. 6 (1996) 15.
[49] G. Kresse, J. Furthmüller, Phys. Rev. B 54 (1996) 11169.
[50] P.E. Blöchl, Phys. Rev. B 50 (1994) 17953.
[51] G. Kresse, D. Joubert, Phys. Rev. B 59 (1999) 1758.
[52] H.J. Monkhorst, J.D. Pack, Phys. Rev. B 13 (1976) 5188.
[53] G. Henkelman, H. Jónsson, J. Chem. Phys. 111 (1999) 7010.
[54] K.J. Laidler, in: Chemical Kinetics, third ed., Harper Collins, New York, 1987. p. 193.
[55] R. van Harrevelt, K. Honkala, J.K. Nørskov, U. Manthe, J. Chem. Phys. 122 (2005) 234702.
[56] A.M. Pessoa, J.L.C. Fajín, J.R.B. Gomes, M.N.D.S. Cordeiro, J. Mol. Struct. (Theochem), submitted for publication.
[57] F. Viñes, A. Borodin, O. Höfft, V. Kempter, F. Illas, Phys. Chem. Chem. Phys. 7 (2005) 3866.
[58] J.L. Ayastuy, M.A. Gutiérrez-Ortiz, J.A. González-Marcos, A. Aranzabal, J.R. González-Velasco, Ind. Eng. Chem. Res. 44 (2005) 41.
[59] J. Rostrup-Nielsen, J.K. Norskov, Topics in Catalysis 40 (2006) 45.
[60] A. Logadottir, J.K. Norskov, J. Catal. 220 (2003) 273.
[61] A. Corma, M. Boronat, S. González, F. Illas, Chem. Commun. (2007) 3371.
[62] G. Wang, L. Jiang, Z. Cai, Y. Pan, X. Zhao, W. Huang, K. Xie, Y. Li, Y. Sun, B. Zhong, J. Phys. Chem. B 107 (2003) 557.
[63] L. Jiang, G.-C. Wang, Z.-S. Cai, Y.-M. Pan, X.-Z. Zhao, J. Mol. Struct. (Theochem) 710 (2004) 97.
[64] J. Ren, S. Meng, J. Am. Chem. Soc. 128 (2006) 9282.
[65] J. Ren, S. Meng, Phys. Rev. B 77 (2008) 054110.
[66] J.L.C. Fajín, M.N.D.S. Cordeiro, J.R.B. Gomes, J. Mol. Struct. (Theochem), in press, doi:10.1016/j.theochem.2009.09.013.
[67] J. Oviedo, R. Sánchez-de-Armas, M.A. San Miguel, J.F. Sanz, J. Phys. Chem. C 112 (2008) 17737.
[68] J.B. Park, J. Graciani, J. Evans, D. Stacchiola, S. Ma, P. Liu, A. Nambu, J.F. Sanz, J. Hrbek, J.A. Rodrigues, Proc. Natl. Acad. Sci. 106 (2009) 4975.
[69] J.K. Nørskov, T. Bligaard, A. Logadottir, S. Bahn, L.B. Hansen, M. Bollinger, H. Bengaard, B. Hammer, Z. Sljivancanin, M. Mavrikakis, Y. Xu, S. Dahl, C.J.H. Jacobsen, J. Catal. 209 (2002) 275.